Avalanches and Scaling in Plastic Deformation

Marisol Koslowski,* Richard LeSar, and Robb Thomson
Theoretical Division, Los Alamos National Laboratory, Los Alamos, New Mexico 87545, USA
(Received 7 April 2004; published 14 September 2004)

Plastic deformation of crystalline materials is a complex nonhomogeneous process characterized by avalanches in the motion of dislocations. We study the evolution of dislocation loops using an analytically solvable phase-field model of dislocations for ductile single crystals during monotonic loading. The distribution of dislocation loop sizes is given by $P(A) \sim A^{-\sigma}$, with $\sigma = 1.8 \pm 0.1$. The exponent is in agreement with those found in acoustic emission experiments. This model also predicts a range of macroscopic behaviors in agreement with observation, including hardening with monotonic loading, and a maximum in the acoustic emission signal at the onset of yielding.

DOI: 10.1103/PhysRevLett.93.125502 PACS numbers: 61.72.Lk, 81.40.Lm, 89.75.Da

Crystalline materials subjected to an external stress display bursts of activity owing to nucleation and motion of dislocations [1–4]. These sudden local changes generate acoustic emission waves that reveal the intermittent and jerky character of dislocation motion.

Acoustic emission (AE) experiments on single crystals of ice under viscoplastic deformation (creep) show that the probability density function of the acoustic emission intensity, $P(A)$, follows a power-law distribution $P(A) \sim A^{-\sigma}$ with an exponent in the range $\sigma \sim 1.6$–2.0 [5]. Self-similarity in dislocation avalanches was also observed spatially; that is, the probability of two avalanches being separated by a distance less than r is given by $C(r) \sim r^{D}$, with $D = 2.5 \pm 0.1$ [6]. Although many acoustic emission measurements have been reported, only qualitative descriptions of the relation with plastic deformation have been made to date.

During plastic deformation in metals, cellular dislocation patterns may develop [7–9]. These patterns consist of dislocation walls separating dislocation-free cell interiors. The presence of fractal patterns of dislocations was first observed in numerical simulations by Sevillano *et al.* [10]. Later, Hähner *et al.* [7] characterized the fractal dimension of the wall structures formed in metals under large deformations. Several analytical models were developed to study the patterning phenomena [7,11–13]. The common feature of these models is that the system is described at a continuum level and the evolution of the dislocation density is described by means of balance equations.

It has been suggested that the dynamics of these systems displays self-organized criticality (SOC) [3,5,6]. Although the concept of self-organized criticality was originated to explain simplified models, phenomena in very diverse field of sciences are said to exhibit SOC. Examples include earthquakes, forest fires, water droplets on surfaces, fracture, and dynamics of magnetic domains in addition to wars and stock market crashes [14].

A rigorous definition and a mathematical formalism of self-organized critical behavior are still lacking. SOC is a phenomenological definition and can be characterized by (i) power-law distributions without any apparent tuning; (ii) the process connected with the external driving of the system needs to be much slower than the internal relaxation processes; (iii) the presence of marginally stable states (Bak *et al.* [15] conceive the marginally stable states as characterized by the lack of any typical length or time scale, related to systems at a critical point); and (iv) a very large number of interacting entities [16].

In this Letter, we present numerical simulations of dislocations that generate scale-free avalanches and power-law behavior in properties related to acoustic emission that are characteristics of SOC. The power-law exponent is in agreement with those found in acoustic emission experiments [5]. This model also predicts a range of macroscopic behaviors in accordance with observation, including hardening with monotonic loading, and a maximum in the acoustic emission signal at the onset of yielding [17–19].

We use a phase-field model of dislocations developed by Koslowski *et al.* [20] in which an integer valued phase-field describes the evolution of dislocation arrangements in single crystals. In this representation the value of the phase field accounts for the number of dislocations which have crossed over a point. Together with the dislocation structures the model predicts the dislocation density. No independent equation of evolution for the dislocation density needs to be supplied, in comparison with other simulations in which nucleation and annihilation mechanisms need to be additionally provided [5].

We consider a system of dislocations moving in a single slip plane through a random array of forest dislocations, under the action of an applied shear stress, which is a good approximation for the stage I of deformation (easy glide) when only a few slip systems are active.

In order to derive the governing equations, we briefly describe a two-dimensional phase-field theory of dislocations. For further details, see Ref. [20]. The model is analytically tractable, which makes it possible to deal with mesoscopic size dislocation ensembles while taking

into account an arbitrary number and arrangement of dislocation lines over a slip plane, the long-range elastic interactions between dislocations, the core structure of the dislocations, the interaction between the dislocations, and an applied shear stress, and the irreversible interactions with short-range point obstacles. The dislocation ensemble is represented by means of a scalar phase field ξ. The phase field is integer valued and its value records the number of dislocations with their sign, which have crossed the point on the slip plane (i.e., the net amount of deformation at that point).

Here, we consider the deformation of an isotropic single crystal during single glide. The system is thus approximated by a single slip plane, which we take to be the (x_1, x_2) plane. We also assume that the Burgers vector, $\boldsymbol{b}$, points in the x_1 direction. Under these assumptions, the energy can be written as [20]

$$E[\xi] = \frac{1}{(2\pi)^2} \int \left(\frac{\mu b^2}{4} \frac{K}{1 + Kd/2} |\hat{\xi}|^2 - \frac{b\hat{\tau}\,\hat{\xi}}{1 + Kd/2} \right) d^2k, \tag{1}$$

where a superimposed $\hat{()}$ denotes a Fourier transform, k_i are the components in the transformed Fourier space of the coordinates x_i, μ is the shear modulus, τ is the applied resolved shear stress, d is the interplanar spacing, and

$$K = \frac{k_2^2}{\sqrt{k_1^2 + k_2^2}} + \frac{1}{1 - \nu} \frac{k_1^2}{\sqrt{k_1^2 + k_2^2}}, \tag{2}$$

where ν is the Poisson's ratio. The first term in Eq. (1) represents the dislocation-dislocation interactions. The second term is the effect of an external applied stress. The operator $\frac{1}{1+Kd/2}$ smoothes the integer valued phase field and appears as a response of the core energy. The nonlocal, long-range dislocation interaction has a similar structure to the functionals used in fluid invasion in porous media and dynamics of ferromagnetic domain walls [21,22].

The slip system contains initially a random distribution of obstacles that represent forest dislocations. Since dislocation motions and reactions are dissipative processes, dislocation patterns resulting from plastic deformation cannot be deduced from minimization principles. The irreversible obstacle interaction is built into the variational formulation by recourse to time discretization. We consider a sequence of discrete times and seek to compute the slip distribution ξ^{n+1} at time t_{n+1}, given the solution ξ^n at time t_n. The updated slip distribution follows from the minimization of the incremental work function:

$$W[\xi^{n+1}|\xi^n] = E[\xi^{n+1}] - E[\xi^n] + \int f(\boldsymbol{x})|\xi^{n+1}(\boldsymbol{x}) - \xi^n(\boldsymbol{x})|d^2x. \tag{3}$$

The last term in (3) is the incremental work of dissipation. In this term, the field $f(\boldsymbol{x}) \geq 0$ represents the energy cost per unit area associated with the passage of one dislocation over the point $\boldsymbol{x}$, i.e., with a transition of the form $\xi(\boldsymbol{x}) \rightarrow \xi(\boldsymbol{x}) \pm 1$. Thus, the field $f(\boldsymbol{x})$ represents the distribution of obstacles over the slip plane and can be represented as [20]

$$f(\boldsymbol{x}) = \sum_i f_i(\boldsymbol{x}), \tag{4}$$

where the sum is over the obstacles and we define the obstacle strength F_i as

$$F_i b^2 = \int f_i(\boldsymbol{x}) d^2x. \tag{5}$$

Equation (3) simply states that part of this work is invested in raising the energy of the crystal, whereas the remainder of the external work supplied is invested in overcoming the obstacle resistance. At each time step the updated configuration corresponds to the minimization of Eq. (3). For the special case of short-range obstacles, the solution can be obtained in closed form, and it results in

$$\xi(\boldsymbol{x}) = P_{\mathbb{Z}}\eta(\boldsymbol{x}), \tag{6}$$

where $P_{\mathbb{Z}}$ is the closest integer projection and $\eta(\boldsymbol{x})$ is the unconstrained solution

$$\eta(\boldsymbol{x}) = \int G(\boldsymbol{x} - \boldsymbol{y}) s(\boldsymbol{x}) d^2y + C, \tag{7}$$

where $G(\boldsymbol{x})$ is the inverse Fourier transform of $1/K$, $s(\boldsymbol{x})$ represents the reaction force field exerted by the obstacles, and C is an integer valued constant.

In the simulations, we consider quasistatic loading in a single slip system containing obstacles of uniform strength in the range $F = 0.2$–$10\ \mu$b with an obstacle density $\rho_{\text{obs}} = 3.8 \times 10^{14}/\text{m}^2$. We assume periodic boundary conditions in a cell of size $0.26\ \mu\text{m}^2$. We set the Poisson's ratio $\nu = 0.3$ and the Burgers vector $b = 2.56 \times 10^{-10}$ m corresponding to copper. At each loading step the solution depends only on the applied stress and the obstacle distribution, and it is obtained in closed form through Eq. (6).

Figure 1 shows the dislocation pattern at an applied stress $\tau = 0.24 \times 10^{-4}\ \mu$ for an obstacle strength $F = \mu$b. Dislocations are identified with lines where the phase field jumps by one. Dislocations move by bowing through

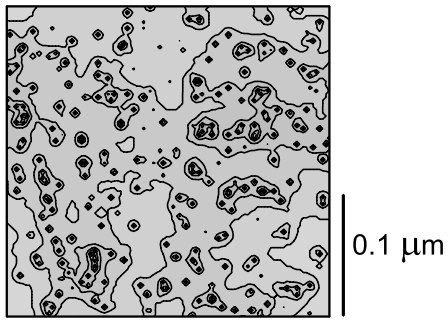

FIG. 1. Dislocation pattern in response to an applied stress $\tau/\mu = 0.24 \times 10^{-4}$.

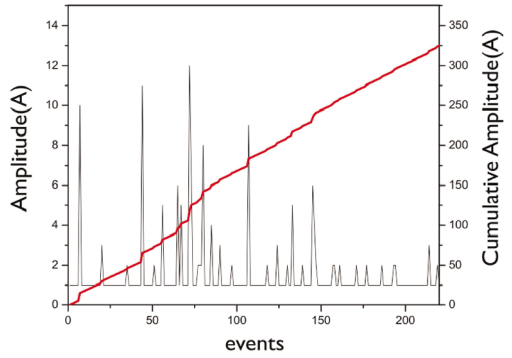

FIG. 2 (color online). Instantaneous and cumulated dislocation activity during one loading step.

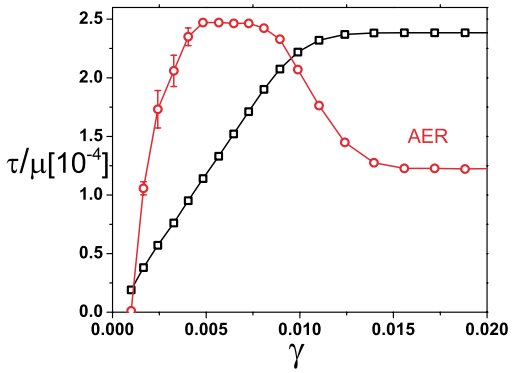

FIG. 3 (color online). Simulated acoustic emission and stress as a function of the slip during monotonic loading.

the open spaces between obstacles leading to the formation of Orowan loops. As the applied stress increases, the number of loops surrounding the obstacles correspondingly increases.

The energy released by the system during one loading step is proportional to the area slipped by the dislocations [3,17,23]. Therefore, the acoustic signal, A, is proportional to the area of the loops generated during one loading step.

Figure 2 shows the calculated acoustic emission amplitude and the cumulative amplitude during one loading step. The AE signal accompanying the plastic deformation consists of many overlapping pulses as observed experimentally in copper and aluminum single crystals [17,19] and ice [3,5]. The instantaneous dissipation shows burst of activity that can be considered dislocation avalanches. The cumulated activity is a measure of the strain and also shows the burst character observed in plastic deformation [1,2]. This behavior also resembles the jerky character of the stress-strain curve observed in alloys, which arises from the interaction of dislocation with solute atoms (Portevin-Le Chatelier effect [4]).

Following [3], we introduce the acoustic emission rate (AER), which measures the acoustic activity during one loading step, i.e., it is the sum of the amplitudes registered during one loading step divided by the duration of the step, t,

$$\mathrm{AER} = \frac{\sum_A N(A)A}{t}, \tag{8}$$

where $N(A)$ is the number of events with amplitude A.

Figure 3 shows the computed stress and the acoustic emission rate as a function of the strain. The signal represents an average over 100 realizations of random distribution of obstacles with the same obstacle density. Error bars in Fig. 3 represent the deviation in the computed stress and AER. Error bars are not shown when are not visible in this scale.

Two well differentiated regimes are clearly present in Fig. 3, a first regime of easy glide or microslip and a second regime characterized by yielding. During the microslip regime, the obstacles are impenetrable; the dislocations move through open spaces leading to the formation of Orowan loops. During this stage, the AER signal shows great dislocation production. At sufficiently large stress, the obstacles yield and are crossed by dislocations, the hardening rate drops, and the stress-strain curve saturates. At the same time the AER, as well as the dislocation production, decrease in agreement with experimental observation [17–19]. The AER signal reduction observed after yielding is attributed to a reduction in the dislocation mean free path due to an increasing dislocation density.

Important information about the statistics of plastic flow can be extracted from the avalanche size distribution. Acoustic emission experiments on single crystals of ice show that the probability density function of the acoustic emission intensity follows a power-law distribution with an exponent in the range $\sigma = 1.6$–2.0 [3,5]. The energy released during one loading step is proportional to the area slipped by the dislocations. Therefore, the acoustic emission intensity is proportional to the area of the dislocation loops generated during loading. Figure 4 shows the simulated loop size probability distribution at three different applied stresses, for random distribution of obstacles with a strength $F = 10\ \mu$b. The distribution exhibits a power-law decay of the form

$$N(A) \sim A^{-\sigma}, \tag{9}$$

with a power-law exponent $\sigma = 1.8 \pm 0.1$ in agreement with experimental observation. Scaling over more than 1 order of magnitude is found and delimited only by finite size effects. The value of the exponent, σ, remains constant (within numerical uncertainties) for the whole range of deformation. We also find in our simulations that the value of the exponent is independent of the obstacle strength and density for a range $F = 0.2$–$10\ \mu$b and $\rho_{\mathrm{obs}} = 1.9$–$3.8 \times 10^{14}/\mathrm{m}^2$, respectively.

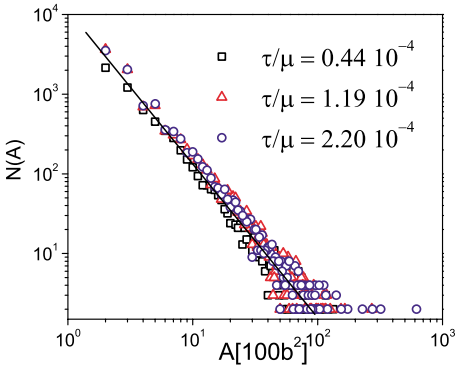

FIG. 4 (color online). Probability distribution $N(A)$ at applied stress $\tau/\mu = 0.44 \times 10^{-4}$, 1.19×10^{-4}, 2.2×10^{-4}.

The numerical simulations of the present model show that plastic deformation under slow external loading occurs in a sequence of avalanches involving the collective motion of many interacting dislocations. The power-law distributions for the AE amplitudes for a wide range of applied stress, the slow driving process, the presence of marginally stable configurations, and the large number of interacting dislocations give further evidence that dislocation dynamics is a new example of a self-organized critical system [3,5].

In addition to the jerky character of dislocation motion, this model also predicts a range of macroscopic behaviors in agreement with observation, including hardening with monotonic loading and a maximum in the AER signal at the onset of yielding. After yielding, the acoustic emission rate decreases in agreement with experiments. In this way, the AER allows the estimation of the production rate of moving dislocations during the plastic deformation of metals.

Because dislocation-driven plastic flow exhibit a scale-free behavior over many decades of sizes, its properties are independent of microscopic and macroscopic details, and great progress can be made by the use of simple models as the present one (universality). In summary, dislocation dynamics involve the collective depinning of a large number of degrees of freedom that are elastically coupled. As such, this model belongs to the class of nonconservative slow-driven systems characterized by scaling laws, in particular, the ones used for earthquakes, fluid invasion in porous media, magnetic systems, and fracture [14,21,24].

The work of M. Koslowski and R. LeSar was performed under the auspices of the United States Department of Energy (U.S. DOE under Contract No. W-7405-ENG-36) and was supported by the Division of Materials Science of the Office of Basic Energy Sciences of the Office of Science of the U.S. DOE. M. K. thanks the Computational Materials Science Network of the US DOE/OS/OBES/DMS for their support.

*Electronic address: marisol@lanl.gov

[1] R. B. Pond, in *The Inhomogeneity of Plastic Deformation* (American Society of Metals, Metals Park, OH, 1973), pp. 1–18.
[2] N. Neuhauser, in *Dislocations in Solids*, edited by F. R. N. Nabarro (North-Holland, Amsterdam, 1983), Vol. 6, p. 321.
[3] J. Weiss and J. R. Grasso, J. Phys. Chem. B **101**, 6113 (1997).
[4] L. P. Kubin, C. Fressengeas, and G. Ananthakrishna, in *Dislocations in Solids*, edited by F. R. N. Nabarro and M. S. Duesbery (North-Holland, Amsterdam, 2002), pp. 101–191.
[5] M. C. Miguel, A. Vespignani, S. Zapperi, J. Weiss, and J. R. Grasso, Nature (London) **410**, 667 (2001).
[6] J. Weiss and D. Marsan, Science **299**, 89 (2003).
[7] P. Hähner, K. Bay, and M. Zaiser, Phys. Rev. Lett. **81**, 2470 (1998).
[8] F. Szekely, I. Groma, and J. Lendvai, Mater. Sci. Eng. A **324**, 179 (2002).
[9] M. Koslowski, R. LeSar, and R. Thomson (to be published).
[10] J. Gil Sevillano, E. Bouchaud, and L. P. Kubin, Scr. Metall. Mater. **25**, 355 (1991).
[11] D. L. Holt, J. Appl. Phys. **41**, 3197 (1970).
[12] L. P. Kubin and G. Canova, Scr. Metall. Mater. **27**, 957 (1992).
[13] I. Groma and B. Bako, Phys. Rev. Lett. **84**, 1487 (2000).
[14] D. L. Turcotte, Rep. Prog. Phys. **62**, 1377 (1997).
[15] P. Bak, C. Tang, and K. Wisenfeld, Phys. Rev. Lett. **59**, 381 (1987).
[16] H. J. Jensen, *Self-Organized Criticality* (Cambridge University Press, Cambridge, England, 1998).
[17] C. Scruby, H. Wadley, and J. E. Sinclair, Philos. Mag. A **44**, 249 (1981).
[18] H. N. G. Wadley and R. Mehrabian, Mater. Sci. Eng. **65**, 245 (1984).
[19] A. Vinogradov, V. Patlan, and S. Hashimoto, Philos. Mag. A **81**, 1427 (2001).
[20] M. Koslowski, A. Cuitiño, and M. Ortiz, J. Mech. Phys. Solids **50**, 2597 (2002).
[21] S. Zapperi, A. Vespignani, and H. Stanley, Nature (London) **388**, 658 (1997).
[22] M. Kardar, Phys. Rep. **301**, 85 (1998).
[23] D. Rouby, P. Fleischmann, and C. Duvergier, Philos. Mag. A **47**, 671 (1983).
[24] J. P. Sethna, K. Dahmen, and C. Myers, Nature (London) **410**, 242 (2001).